Desalination and Water Treatment
www.deswater.com

47 (2012) 130–138
September

doi: 10.1080/19443994.2012.696826

Taylor & Francis
Taylor & Francis Group

Preparation and characterization of activated carbon from melon (*Citrullus vulgaris*) seed hull by microwave-induced NaOH activation

K.Y. Foo, B.H. Hameed*

School of Chemical Engineering, Engineering Campus, Universiti Sains Malaysia, 14300 Nibong Tebal, Penang, Malaysia
Tel. +60 45996422; Fax: +60 45941013; email: chbassim@eng.usm.my

Received 12 September 2011; Accepted 6 March 2012

ABSTRACT

In the present work, melon seed hull (MS), an industrial effluent abundantly available from the melon seed oil processing plants was utilized as a feedstock for preparation of activated carbon (MSAC) by microwave assisted NaOH chemical activation. MSAC was characterized by Fourier transform infrared spectroscopy, scanning electron microscopy, elemental analysis, and nitrogen adsorption–desorption study. The adsorptive properties of MSAC were quantified using methylene blue (MB), cationic dye, and acid blue 15 (AB); anionic dye as model adsorbates. The surface chemistry was examined by zeta potential measurement and evaluation of surface acidity/basicity. Result showed that the monolayer adsorption capacities of MSAC for MB and AB were 333.50 and 341.96 mg/g, respectively. The BET surface area, Langmuir surface area, and total pore volume of MSAC were identified to be 1,187 m^2/g, 1,804 m/g, and 0.68 cm^3/g, respectively. The findings revealed the potential use of MS derived activated carbon for cationic and anionic dyes removal.

Keywords: Activated carbon; Adsorption; Dye; Isotherm; Melon seed hull; Microwave

1. Introduction

By nature, watermelon is a vine-like (scrambler and trailer) flowering plant belonging to the family Cucurbitaceous and genus of *Catullus* [1]. Its fruit is primarily eaten fresh and available as food complements in desserts, salads, fruits cocktail, jam, or juice combinations [2]. Melon seed oil is a popular condiment in the manufacturing of margarines, shortenings, and cooking oils, and the residual cake has been consumed as a valuable source of protein [3]. Traditionally, melon seed oil is extracted by sequential steps of shelling, cleaning, cooking, and grinding [4]; while for larger production, the use of screw and hydraulic press, which requires size reduction of the melon seeds, followed by heat treatment, and application of great pressure is implemented [5].

The refining process, however, is accompanied by the co-production of lignocellulosic biomass in the form of melon seed hull (MS), which comprises 50% of the melon seeds. In the formal practice, some quantity of this residue is used as boiler fuel, where major portion is discarded by open burning. This urged research towards upgrading of the available biomass from the oil refineries. To the best of our knowledge, no study has been reported on the preparation of

*Corresponding author.

activated carbon from MS by microwave-induced activation. The aforementioned study was undertaken to evaluate the viability of microwave irradiation for preparation of activated carbon from MS by NaOH activation. Structural, functional, and elemental characterization of the prepared adsorbent was performed. Moreover, the surface chemistry and adsorption equilibrium of both cationic methylene blue (MB) and anionic acid blue 15 (AB) dyes were outlined.

2. Materials and methods

2.1. Adsorbate

MB and AB, the cationic and anionic pollutants difficult to be degraded in natural environment were chosen as the targeted adsorbates in this study. The standard stock solution was prepared by dissolving an accurate amount of dye in deionized water. The experimental solution was obtained by diluting the stock solution in accurate proportions to different initial concentrations.

2.2. Preparation of activated carbon

Locally obtained MS was the precursor used in the present study. The raw precursor was cleaned with deionized water, dried at 110°C for 48 h, and crushed to obtain the particle size of 1–2 mm. The carbonization process was performed by loading the dried precursor into a muffle furnace and heated up to a carbonization temperature of 700°C, under nitrogen gas flow (150 cm^3/min).

The determination of the best activation conditions was based on the highest yield and adsorption uptake as reported elsewhere [6]. The char produced was mixed with sodium hydroxide (NaOH) solution in a (NaOH:char) ratio of 1:1.25 (wt.%). The activation step was performed in a glass reactor, placed in a modified microwave oven with a frequency of 2.45 GHz [6]. The microwave power was set to 600 W and 7 min of irradiation time was selected as the heating period based on preliminary runs. The resulting sample was washed with 0.1 M of HCl and rinsed repeatedly with hot and cold deionized water until the pH of the washing solution reached 6–7.

2.3. Characterization of MSAC

Scanning electron microscopy (SEM) analysis was carried out to study the surface morphologies of char and MSAC. The pore structural characteristics were characterized by nitrogen adsorption at 77 K using an automatic volumetric adsorption analyzer (Micromeritics ASAP-2020). Surface functional groups and elemental analysis were detected by Fourier transform infrared (FTIR) spectroscope (FTIR-2000, PerkinElmer) by scanning in the range of 4,000 to 400 cm^{-1} and elemental analyzer (EA-2400 Series II, PerkinElmer).

2.4. Surface acidity and basicity

The surface basicity was estimated by mixing 0.2 g of MSAC with 25 mL of (0.05 M) HCl solution in a closed flask, and agitated for 48 h at room temperature. The suspension was decanted and the remaining HCl was titrated with 0.05 M of NaOH solution. The surface acidity was measured by titration with 0.05 M of HCl after incubation 0.2 g of MSAC with 0.05 M of NaOH solution.

2.5. Zeta potential measurement (pH_{pzc})

The determination of the pH_{pzc} was conducted by adjusting the pH of 50 cm^3 by 0.01 M of NaCl solution to a value between 2 and 12. MSAC of 0.15 g was added and the final pH was measured after 48 h under agitation. The pH_{pzc} is the point where $pH_{final} - pH_{inital} = 0$.

2.6. Adsorption equilibrium studies

Adsorption equilibrium studies were conducted in a set of 250 mL conical flasks containing 0.20 g adsorbent and 200 mL dye solutions with various initial concentrations (50, 100, 200, 300, 400, and 500 mg/L). The flasks were agitated in an isothermal water bath shaker at 120 rpm at 30°C for 24 h until the equilibrium was reached. All samples were filtered to minimize the interference of carbon fines with the analysis. Each experiment was duplicated under identical conditions. MB/AB uptake at equilibrium, q_e (mg/g), was calculated by Eq. (1):

$$q_e = \frac{(C_0 - C_e)V}{W} \quad (1)$$

where C_0 and C_e (mg/L) are the liquid-phase concentrations of dye at initial and equilibrium, respectively. V (L) is the volume of the solution and W (g) is the mass of adsorbent used. The effect of pH on MB/AB removal was tested by varying the pH from 2 to 12, with initial MB concentration of 500 mg/L, MSAC dosage of 0.20 g/200 mL, and adsorption temperature of 30°C.

2.7. Adsorption isotherm

Adsorption isotherms express the specific relation between adsorbate concentration in the bulk and adsorbed amount at the interface. Due to the inherent bias resulting from linearization, alternative isotherm parameter sets were determined by nonlinear regression [7]. This provides a mathematically rigorous method for determining isotherm parameters using the original form of isotherm equations. The equilibrium data were fitted to the nonlinear Freundlich [8], Langmuir [9], Temkin [10], and Redlich–Peterson [11] isotherm models derived as:

$$q_e = K_F C_e^{1/n} \tag{2}$$

$$q_e = \frac{Q_0 K_L C_e}{1 + K_L C_e} \tag{3}$$

$$q_e = B \ln(A C_e) \tag{4}$$

$$q_e = \frac{K_R C_e}{1 + a_R C_e^g} \tag{5}$$

where K_F (mg/g) $(L/mg)^{1/n}$ and $1/n$ are the Freundlich adsorption constant and a measure of adsorption intensity; Q_0 (mg/g) and K_L (L/g) are Langmuir isotherm constants related to adsorption capacity and energy of adsorption. Meanwhile, $B = RT/b$, with b (J/mol), A (L/g), R (8.314 J/mol K), and T (K) are Temkin isotherm constant related to heat of sorption, equilibrium binding constant, gas constant, and absolute temperature; where K_R (L/g) and a_R $(1/mg)^g$ are Redlich–Peterson isotherm constants, and g is the isotherm exponent.

3. Results and discussion

3.1. Textural and surface characterization

Nitrogen adsorption isotherm provides qualitative information on the adsorption mechanism and porous structure of the carbonaceous materials [12]. The nitrogen adsorption–desorption plot of MSAC is shown in Fig. 1(a). The isotherm pertains an intermediate between type I and type II isotherm as defined by the International Union of Pure and Applied Chemistry (IUPAC) classification, which associated with a combination of microporous and mesoporous structures. The specific surface area (S_{BET}) was calculated by the BET equation; the total pore volume (V_T) was evaluated by converting the adsorption volume of nitrogen at relative pressure 0.95 to equivalent liquid volume of the adsorbate, while the external and micropore surface areas were deduced from the *t*-plot method. These surface physical parameters obtained from the nitrogen adsorption isotherm were summarized in Table 1. From the data, it can be inferred that the porosity of MSAC was greatly improved, indicating pore development during the activation stage. Mean-

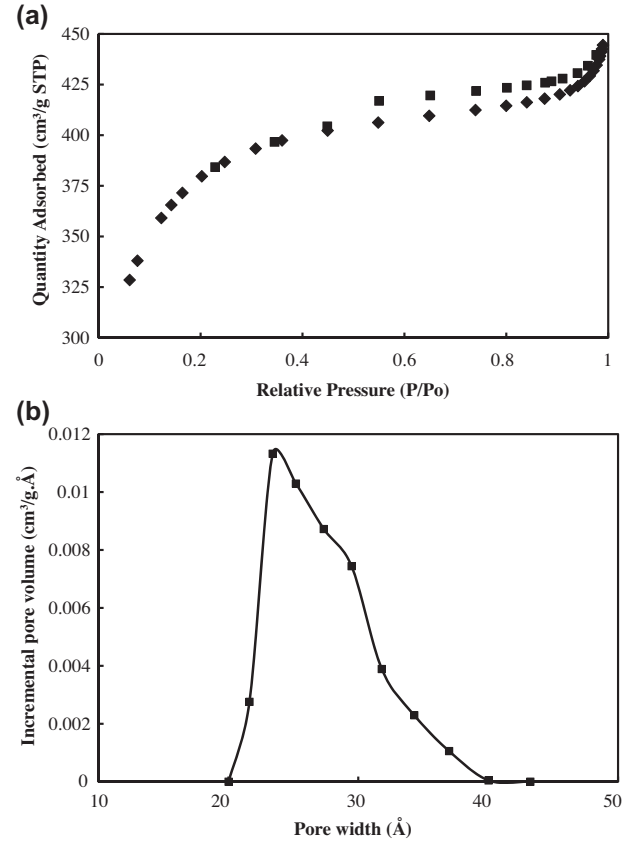

Fig. 1. Nitrogen adsorption–desorption (a) and pore size distribution (b) curves of MSAC.

Table 1
Porosity structures of the MS derived char and MSAC

Properties	Char	MSAC
BET surface area (m^2/g)	69	1,187
Micropore surface area (m^2/g)	48	671
External surface area (m^2/g)	21	516
Langmuir surface area (m^2/g)	102	1,804
Total pore volume (cm^3/g)	0.04	0.68
Micropore volume (cm^3/g)	0.02	0.36
Mesopore volume (cm^3/g)	0.02	0.32
Average pore size (Å)	24.07	22.90

while, it was evident that the mesopores of MSAC accounts about 47% of the total pore volume, with a well-developed porous structure.

The pore size distribution of WSAC was ascertained by density functional theory (DFT) model. According to the classification of IUPAC-pore dimensions, the pores of adsorbents are grouped into micropore ($d < 2$ nm), mesopore ($d = 2$–50 nm), and macropore ($d > 50$ nm) [13]. The graph (Fig. 1(b)) detected the sharpest peak at pore diameter between 2 and 5 nm, with an average pore size of 22.90 Å, which shows that a majority of the pores fall into the range of mesopore.

The morphological structure of the MS derived char and MSAC is depicted in Fig. 2. It can be found that the surface of the primary char was dense, planar, and blocked by deposited tarry substances. However, the microwave irradiated sample demonstrated a well-developed porous surface, forming an orderly pore structure. Comparison of the surface morphology verifies substantial changes occasioned by microwave irradiation.

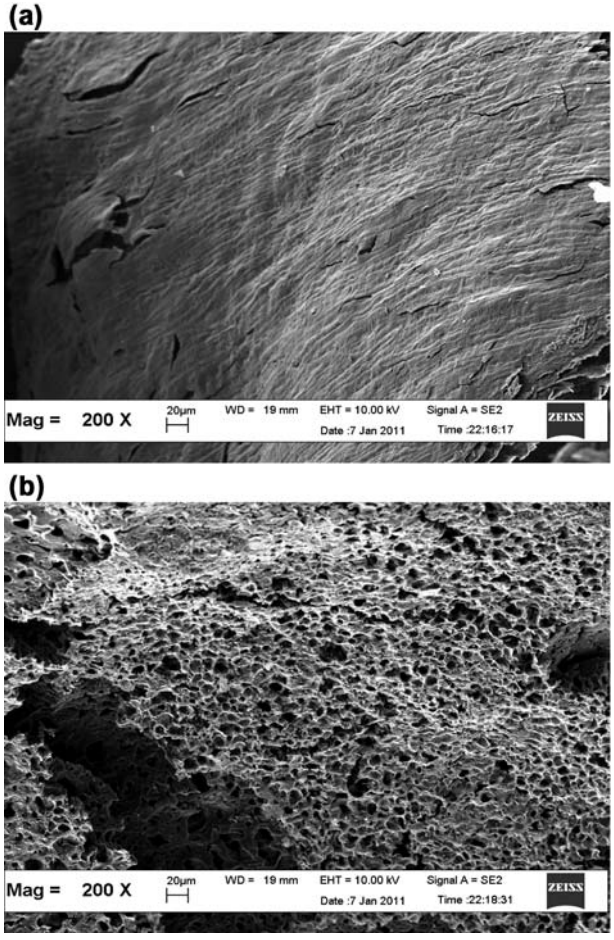

Fig. 2. SEM micrographs of the MS derived char (a) and MSAC (b).

It can be deduced that the pore enlargement related to NaOH activation is associated to the redox reduction and oxidative modification responsible for the development of micro and mesoporosity. During the reaction, the evolution of CO, CO_2, and H_2 constituents, and additional reactions [14] between the active intermediates with the carbon surface were possible. Concurrently, the alkaline and carbonate metal formed during the activation stage were intercalated to the carbon matrix responsible for both stabilization and widening of pores between the carbon atomic layers.

3.2. Elemental and functional characterization

The chemical composition of char and MSAC was listed in Table 2. The carbon level increased after microwave treatment, but the content of oxygen, hydrogen, and nitrogen indicated an opposite trend. This is due to the elimination of oxygen-containing groups and decomposition of volatiles compounds under microwave irradiation leaving a high purity carbon. Whereas, the sulfur remaining groups in the carbonized char were thermally stable.

Representative FTIR spectra of char and MSAC were presented in Fig. 3. The broad band at 3,234/3,233 cm^{-1} was related to the in-plane –OH (hydroxyl) groups, and the region between 1,646 cm^{-1} was ascribed to the C=C stretch of alkenes. The signal at 1,425 cm^{-1} was assigned to the $–CH_2$ (alkyl), while intensities at 1,276 and 1,053 cm^{-1} were corresponding to the vibration of C–O–C (ester, ether, and phenol) and C–O (anhydrides) structures. Similarly, the presence of out-of-plane O–H (hydroxyl) groups shows the transmittance at 940 cm^{-1}, and the peaks at 829 and 618 cm^{-1} were associated with the out-of-plane N–O and C–H (alkynes) functional groups. For MSAC, the elimination and shift of peaks were indicative of the modification of surface chemistry by microwave irradiation.

Table 2
Elemental analysis of char and MSAC

Analysis		Char	MSAC
Element (wt.%)	Carbon	51.90	70.13
	Oxygen	43.68	26.77
	Hydrogen	3.83	2.66
	Nitrogen	0.42	0.28
	Sulfur	0.17	0.16

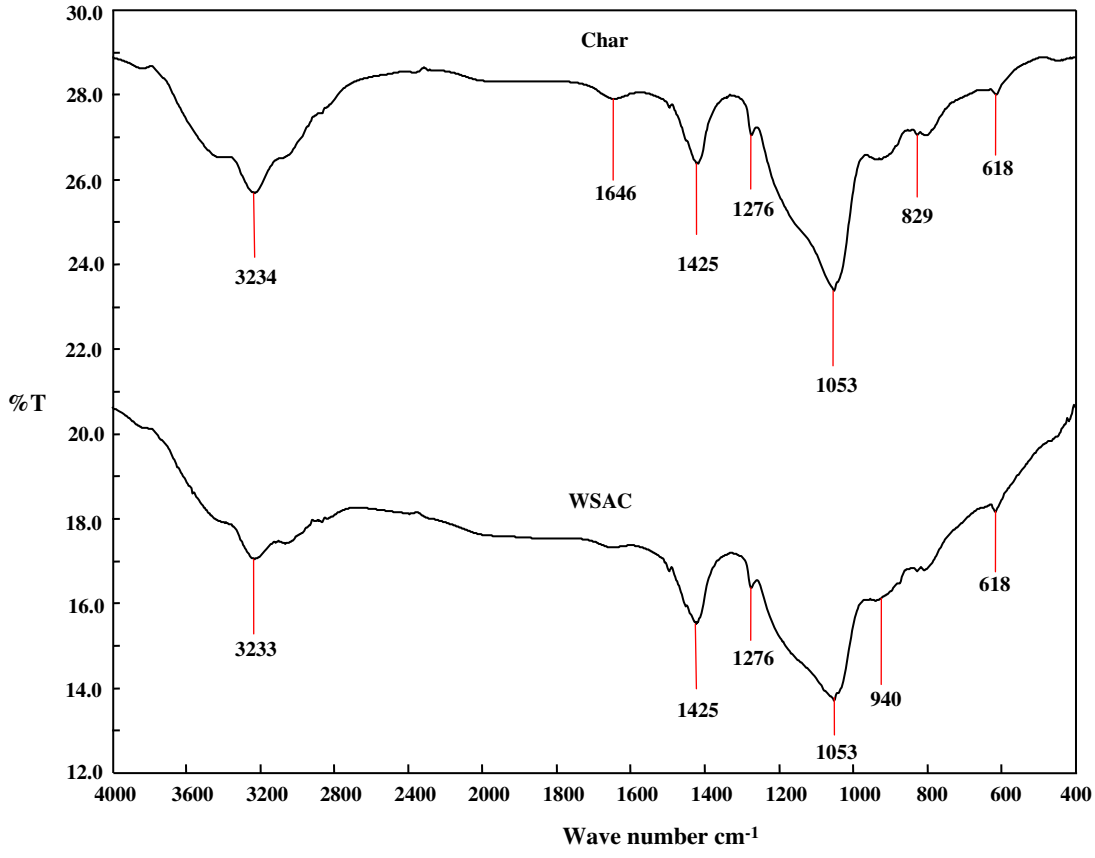

Fig. 3. FTIR spectra of the MS derived char and MSAC.

The surface acidity and basicity is an important criterion describing the surface chemistry of the carbon adsorbents [15]. MSAC showed an amphoteric property, with a surface acidity of 0.95 mmol/g and a surface basicity as 0.94 mmol/g. From the result, it is well established that there are equal amounts of oxygen-containing groups (mainly carboxylic, anhydrides, lactones, and phenols) and oxygen-free Lewis sites, carbonyls, pyrone, and chromene type structures at the edge of the carbon layers. The surface chemistry of MSAC was further justified by determination of zero point of charge (pH_{ZPC}), an index of the propensity of surface charge as a function of pH [16] using the acid/base titration method. The pH_{ZPC} was found to be 7.14.

3.3. Adsorption equilibrium studies

The adsorptive properties of MSAC were evaluated using AB and MB, usually adopted as anionic and cationic adsorbates for commercial ACs. The curve adsorption equilibrium, q_e vs. equilibrium concentration, C_e for both dyes is shown in Fig. 4(a). The adsorption equilibrium of AB and q_e increased from 50.36 to 340.78 mg/g, with an increase in initial concentration from 50 to 500 mg/L. Similar observation was illustrated by the adsorption equilibrium of MB onto MSAC (from 50.21 to 331.20 mg/g), mainly attributed to the driving force of the concentration gradient between aqueous phase and the solid medium [17].

Solution pH affects adsorption by regulating the adsorbents surface charge as well as degree of ionization of the adsorbate molecules [18]. The adsorption behavior of MB and AB over a broad pH range of 2–12 was depicted in Fig. 4(b). Increase in solution pH exerted a significant enhancement of the adsorption uptake of MB from 365.44 to 487.37 mg/g, mainly ascribed to the protonation of MB in the acidic medium, and the presence of excess H^+ ions, competing with dye cations for adsorption sites. At higher solution pH, the formation of electric double layer changes the polarity and consequently, the dye uptake increases. Meanwhile, the uptake of AB increased proportional to the decrease of pH from 310.22 to

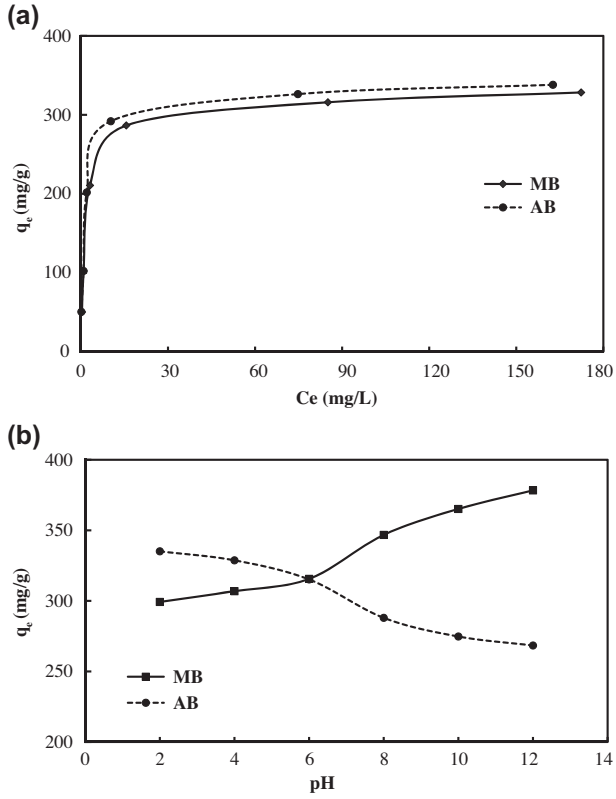

Fig. 4. Adsorption equilibrium (a) and effect of pH (b) on the adsorption of MB and AB onto MSAC at 30˚C.

475.09 mg/g, primarily due to the association of dye anions with the positively charged sites of MSAC. In the basic conditions, electrostatic repulsion exists between the negatively charged surface and dye molecules, thus decrease the adsorption capacity.

Effect of the pH can be described on the basis of zero point of charge (pH_{ZPC}), the point which the net charge of adsorbent is zero. The experimental determination of pH_{ZPC} of MSAC has been identified to be 7.14. When solution $pH < pH_{ZPC}$, activated carbon adsorbent will react as a positive surface; and it will react as a negative surface when the solution $pH > pH_{ZPC}$ [19]. Therefore, for the pH values above 7.14, the negative charge density of MSAC increases, which favors the adsorption of cationic dye. Conversely, for $pH < 7.14$, the surface functional groups on the carbon were protonated, thus enhanced the adsorption of anionic dye molecules.

3.4. Isotherm modeling

In this study, the nonlinear Freundlich, Langmuir, Temkin, and Redlich–Peterson isotherm models were established. A comparison between the experimental data points and the theoretical isotherms plot is displayed in Fig. 5. The detailed parameters of these different forms of isotherm equations are listed in Table 3. The equilibrium data were getting valid for Langmuir isotherm model, while Freundlich and Temkin isotherms do not well represent the adsorption data. The applicability of Langmuir isotherm model suggests that the adsorption process is monolayer with each molecule posing equal enthalpy and activation energy. The results demonstrated no interaction and transmigration of dyes in the plane of the neighboring surface. The suitability of Langmuir isotherm to fit the data was verified by the exponent value of Redlich–Peterson isotherm model, g, which approximate to unity, resulted to the original Langmuir equation.

The essential feature of Langmuir isotherm can be expressed in terms of separation factor, R_L, a dimensionless constant defined as:

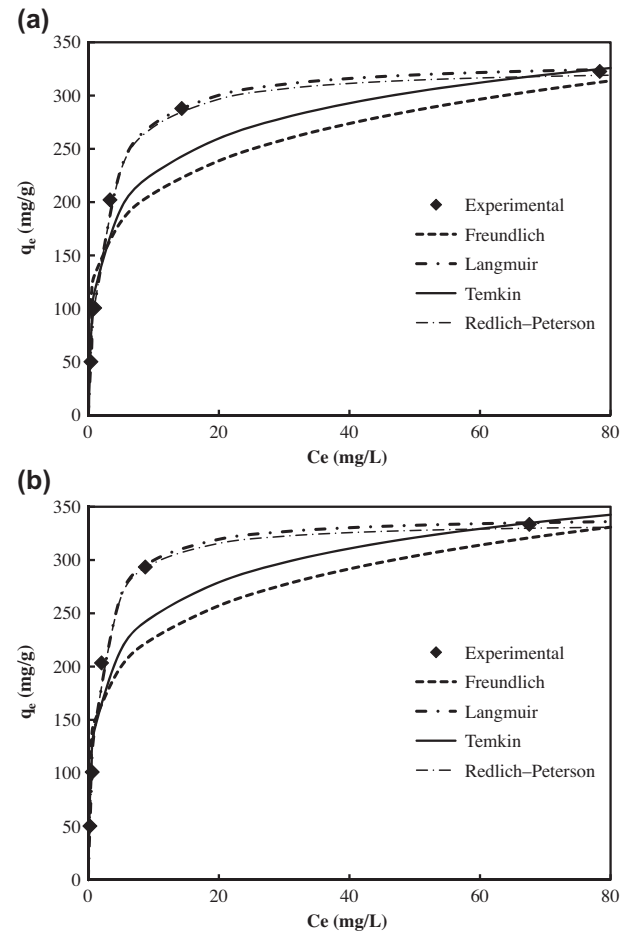

Fig. 5. Adsorption isotherm for the adsorption of MB (a) and AB (b) onto MSAC at 30˚C.

Table 3
Isotherm parameters for the adsorption of AB and MB onto MSAC at 30°C

Isotherm model		Adsorbates	
		AB	MB
Langmuir	Q_o (mg/g)	341.96	333.50
	b (L/mg)	0.71	0.45
	R^2	0.999	0.999
Freundlich	K_F (mg/g).(L/mg)$^{1/n}$	149.14	132.24
	n	5.50	5.07
	R^2	0.825	0.803
Temkin	A (L/g)	22.30	11.68
	B	45.75	47.64
	R^2	0.923	0.937
Redlich–Peterson	a_R (1/mg)^g	0.72	0.46
	K_R (L/g)	244.40	152.13
	g	0.998	1.001
	R^2	0.999	0.997

$$R_L = \frac{1}{1 + K_L C_0} \tag{6}$$

where R_L indicates isotherm to be either unfavorable ($R_L > 1$), linear ($R_L = 1$), favorable ($0 < R_L < 1$), or irreversible ($R_L = 0$). From Fig. 6, it is clearly revealed that

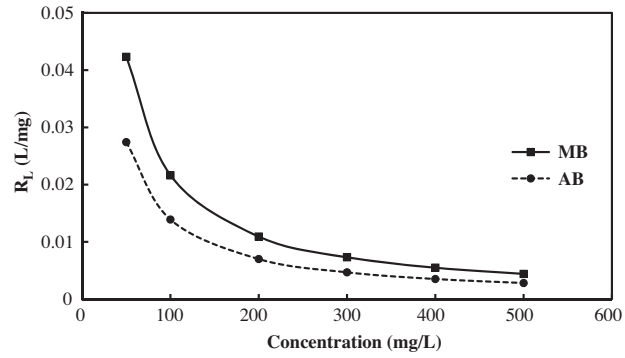

Fig. 6. Effect of initial concentration on the separation factor, R_L.

Table 4
Comparison adsorption capacities of various activated carbons for AB and MB

Precursor	Activation method	Activating agent	Activation time (min)	Adsorption capacity (mg/g)		Reference
				Methylene blue	Acid blue	
MS	Microwave heating	NaOH	7	333.50	341.96	Present study
Rice husk	Microwave heating	K_2CO_3	7	441.52		[20]
Spent catalysts of vinyl synthesis	Microwave heating	Steam	40	285.00		[21]
Pistachio nut shells	Microwave heating	KOH	7	296.57		[22]
Date stone	Microwave heating	KOH	8	316.11		[23]
Posidonia oceanica (L.) dead leaves	Conventional heating	$ZnCl_2$	120	285.70		[24]
Rice straw	Conventional heating	$(NH_4)_2HPO_4$	120	129.50		[25]
Waste rubber tire	Conventional heating	H_2O_2	1,440		9.20	[26]
Coconut coir pith	Conventional heating	N_2	60		15.24	[27]
Pine cone	Conventional heating	H_3PO_4	60		298.40	[28]
Sugar cane bagasse	Conventional heating	H_2SO_4–CO_2	600		217.40	[29]
Hemp bast	Conventional heating	H_3PO_4	120		28.75	[30]

the adsorption process was favorable at the concentrations range being studied. Increasing concentration from 50 to 500 mg/L demonstrated a gradual decrease in R_L, indicating that higher initial dye concentration may enhance the sorption process.

Table 4 summarizes a comparison of maximum monolayer adsorption capacity of various activated carbons derived from different precursors [20–30]. It can be concluded that the activated carbon prepared in this work showed relatively high adsorption capacity of 330.96 and 339.58 mg/g for MB and AB, respectively, as compared to the literature. Thus, it is noteworthy that considerable changes in the surface properties were achieved within a short time, which should be attributed to the distinct mechanism of microwave heating. The activation time due to present work is much shorter owing to the thermal efficiency of microwave heating system. In conventional heating, the energy is transferred by conduction and convection, which results in a thermal gradient reducing from the surface to the inside. However, microwave radiation promotes volumetric heating, leading to a thermal gradient opposite to conventional heating [31]. This irradiation has promoted the release of volatiles from the char surface widening the porosity in the original carbon network. The main advantage of using microwave heating is that the treatment time can be considerably reduced, which in many cases represents a reduction in consumption of gases as well. Additionally, microwave-induced activation may react effectively at lower bulk temperatures, resulting in energy and cost savings [32].

4. Conclusion

The results revealed the viability to prepare activated carbon from MS by microwave-induced NaOH activation. The activation process took 7 min at the operating power of 600 W. Microwave heating has successfully reduced the activation time, which represents the reduction of energy and cost as well. Experimental data were best described by the Langmuir isotherm model, showing a maximum monolayer adsorption capacity of 333.50 and 341.96 mg/g for MB and AB, respectively.

Acknowledgment

The authors acknowledge the financial support provided by Universiti Sains Malaysia under the Research University (RU) Scheme (Project No. 1001/PJKIMIA/814072) and RU-PRGS grant scheme (Project 465 No. 8043030).

References

[1] S.F.F. Ribeiro, A.P. Agizzio, O.L.T. Machado, A.G.C.N. Ferreira, M.A. Oliveira, K.V.S. Fernandes, A.O. Carvalho, J. Perales, V.M. Gomes, A new peptide of melon seeds which shows sequence homology with vicil: partial characterization and antifungal activity, Sci. Hortic. 111 (2007) 399–405.
[2] T.C. Wehner, Watermelon, In: J. Prohens, F. Nuez (Eds), Handbook of plant breeding; vegetables I: asteraceae, brassicaceae, chenopodiaceae, and cucurbitaceae, Springer Science Business LLC, New York, NY, 2008, pp. 381–418.
[3] O.O. Ajibola, S.E. Eniyemo, O.O. Fasina, K.A. Adeeko, Mechanical expression of oil from melon seeds, J. Agric. Eng. Res. 45 (1990) 45–53.
[4] V.A. Oyenuga, B.A. Fetuga, Some aspects of the biochemistry and nutritional value of the water melon seed, J. Sci. Food Agric. 26 (1975) 843–854.
[5] L.M. Khan, M.A. Hanna, Expression of oil from oilseeds—a review, J. Agric. Eng. Res. 28 (1983) 495–503.
[6] K.Y. Foo, B.H. Hameed, Microwave-assisted preparation and adsorption performance of activated carbon from biodiesel industry solid reside: influence of operational parameters, Bioresour. Technol. 103 (2012) 398–404.
[7] K.Y. Foo, B.H. Hameed, Insights into the modeling of adsorption isotherm systems, Chem. Eng. J. 156 (2010) 2–10.
[8] H. Freundlich, Über die adsorption in lösungen (adsorption in solution), Z. Phys. Chem. 57 (1906) 384–470.
[9] I. Langmuir, The adsorption of gases on plane surfaces of glass, mica and platinum, J. Am. Chem. 57 (1918) 1361–1403.
[10] M.I. Tempkin, V. Pyzhev, Kinetics of ammonia synthesis on promoted iron catalyst, Acta Phys. Chim. USSR 12 (1940) 327–356.
[11] O. Redlich, D.L. Peterson, A useful adsorption isotherm, J. Phys. Chem. 63 (1959) 1024–1026.
[12] M. Belhachemi, F. Addoun, Adsorption of congo red onto activated carbons having different surface properties, studies of kinetics and adsorption equilibrium, Desalin. Water Treat. 37 (2012) 122–129.
[13] N. Bouchemal, F. Addoun, Adsorption of dyes from aqueous solution onto activated carbons prepared from date pits: the effect of adsorbents pore size distribution, Desalin. Water Treat. 7 (2009) 242–250.
[14] E.R. Piñero, P. Azaïs, T. Cacciaguerra, D.C. Amorós, A.L. Solano, F. Béguin, KOH and NaOH activation mechanisms of multiwalled carbon nanotubes with different structural organization, Carbon 43 (2005) 786–795.
[15] S. Gammoudi, N.F. Srasra, M.A. Goncalves, E. Srasra, Acid-base and adsorptive properties of Tunisian Smectite, Desalin. Water Treat. 26 (2011) 266–278.
[16] C.Y.Y. Tang, Y.J. Peng, Fouling of ultrafiltration membrane during secondary effluent filtration, Desalin. Water Treat. 30 (2011) 289–294.
[17] K.Y. Foo, B.H. Hameed, An overview of dye removal via activated carbon adsorption process, Desalin. Water Treat. 19 (2010) 255–274.
[18] J.M. Abdul, S. Vigneswaran, W.G. Shim, J. Kandasamy, Fouling of ultrafiltration membrane during secondary effluent filtration, Desalin. Water Treat. 30 (2011) 289–294.
[19] K.Y. Foo, B.H. Hameed, Factors affecting the carbon yield and adsorption capability of the mangosteen peel activated carbon prepared by microwave assisted K_2CO_3 activation, Chem. Eng. J. 180 (2012) 66–74.
[20] K.Y. Foo, B.H. Hameed, Utilization of rice husks as a feedstock for preparation of activated carbon by microwave induced KOH and K_2CO_3 activation, Bioresour. Technol. 102 (2011) 9814–9817.
[21] Z.Y. Zhang, W.W. Qu, J.H. Peng, L.B. Zhang, X.Y. Ma, Z.B. Zhang, W. Li, Comparison between microwave and conventional thermal reactivations of spent activated carbon generated from vinyl acetate synthesis, Desalination 249 (2009) 247–252.

[22] K.Y. Foo, B.H. Hameed, Preparation and characterization of activated carbon from pistachio nut shells via microwave-induced chemical activation, Biomass Bioenergy 35 (2011) 3257–3261.
[23] K.Y. Foo, B.H. Hameed, Preparation of activated carbon from date stones by microwave induced chemical activation: application for methylene blue adsorption, Chem. Eng. J. 170 (2011) 338–341.
[24] M.U. Dural, L. Cavas, S.K. Papageorgiou, F.K. Katsaros, Methylene blue adsorption on activated carbon prepared from *Posidonia oceanica* (L.) dead leaves: kinetics and equilibrium studies, Chem. Eng. J. 168 (2011) 77–85.
[25] P. Gao, Z.H. Liu, G. Xue, B. Han, M.H. Zhou, Preparation and characterization of activated carbon produced from rice straw by $(NH_4)_2HPO_4$ activation, Bioresour. Technol. 102 (2011) 3645–3648.
[26] V.K. Gupta, B. Gupta, A. Rastogi, S. Agarwal, A. Nayak, A comparative investigation on adsorption performances of mesoporous activated carbon prepared from waste rubber tire and activated carbon for a hazardous azo dye—Acid Blue 113, J. Hazard. Mater. 186 (2011) 891–901.
[27] D. Kavitha, C. Namasivayam, Capacity of activated carbon in the removal of acid brilliant blue: determination of equilibrium and kinetic model parameters, Chem. Eng. J. 139 (2008) 453–461.
[28] M. Hadi, M.R. Samarghandi, G. McKay, Equilibrium two-parameter isotherms of acid dyes sorption by activated carbons: study of residual errors, Chem. Eng. J. 160 (2010) 408–416.
[29] M. Valix, W.H. Cheung, G. McKay, Sulfur fixation on bagasse activated carbon by chemical treatment and its effect on acid dye adsorption, Adsorption 15 (2009) 453–459.
[30] R. Yang, G.Q. Liu, X.H. Xu, M. Li, J.C. Zhang, X.M. Hao, Surface texture, chemistry and adsorption properties of acid blue 9 of hemp (*Cannabis sativa* L.) bast-based activated carbon fibers prepared by phosphoric acid activation, Biomass Bioenergy 35 (2011) 437–445.
[31] B.V. Sánchez, New insights in vulcanization chemistry using microwaves as heating source, Ph.D. thesis, Department of Industrial Engineering Institut Químic de Sarrià, University Ramon Llull, 2008.
[32] K.Y. Foo, B.H. Hameed, Recent developments in the preparation and regeneration of activated carbons by microwaves, Adv. Colloid Interface Sci. 149 (2009) 19–27.